Engineering Structures 272 (2022) 114586

Contents lists available at ScienceDirect

Engineering Structures

journal homepage: www.elsevier.com/locate/engstruct

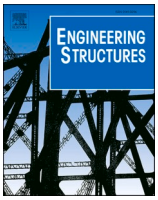

Integrity monitoring of cast in-situ piles using thermal approach: A field case study

Qianchen Sun [a], Mohammed Z.E.B. Elshafie [b], Chris Barker [c], Anthony Fisher [d], Jennifer Schooling [a], Yi Rui [e,*]

[a] Centre for Smart Infrastructure and Construction, Department of Engineering, University of Cambridge, Cambridge, UK
[b] Department of Civil and Architectural Engineering, Qatar University, Doha, Qatar
[c] Ove Arup and Partners Ltd, London, UK
[d] Cementation Skanska Ltd, UK
[e] College of Civil Engineering, Tongji University, Shanghai, China

ARTICLE INFO

Keywords:
Thermal integrity test
Pile anomaly detection
Finite element modelling
Cast in-situ pile
Structural health monitoring
Non-destructive test

ABSTRACT

A review of the literature shows that pile integrity is a significant concern in pile construction; in particular, determining the location and nature of anomalies along the depth of the piles using thermal integrity testing data. This paper proposes a new anomaly detection approach which combines early-age temperature monitoring data and finite element back-analyses. A case study on a continuous flight auger (CFA) test pile with engineered inclusions was conducted using this new approach. Through 1D finite element analysis, a linear relationship between maximum temperature and effective pile radius is established. A crucial indicator – 'the effective pile radius' could be used to reconstruct as-built pile 3D shape and identify anomalous regions inside or outside the pile reinforcement cage. The data interpretation results of the field case study show that thermal integrity testing provides reliable information to identify anomalous regions within the pile. Compared to the conventional cross-hole sonic logging, thermal integrity testing used in combination with the new approach presented in this paper, can provide more reliable information in the pile integrity assessment process.

1. Introduction

Pile foundations are widely used in construction due to their ability to overcome poor soil conditions by transferring the imposed loads deep into stronger and stiffer soils and hence avoiding the softer soils closer to the surface. The growing use of pile foundations, however, highlights the challenges associated with pile construction. The difficulty of in-situ pile quality assessment is one such challenge; potential shaft instability and difficult conditions for visual inspection [32] present additional challenges for quality checks. Pile integrity testing aims to address this problem by detecting defects inside piles following their construction.

Current pile integrity tests can be categorised into destructive and non-destructive tests. The destructive test is based on the partial or complete drilling and extraction of the foundation piles. It is a highly informative method but is impractical for most construction projects because it is costly and time-consuming. The commonly used method in industry is non-destructive integrity testing, which includes cross-hole sonic logging (CSL), sonic echo testing (SET), radiation-based gamma-gamma logging (GGL) and pre-construction pile load testing [33,7,14,25,24]. Unfortunately, current non-destructive test methods for pile integrity are still not fully reliable [8]. Failure to detect defects and the occurrence of false positives remain common across various testing systems [14]. For example, uncured concrete and de-bonding can influence the results of CSL. The proximity of steel reinforcement could influence results by absorbing radiation of GGL and the ground stiffness limits the testing depth of SET. Another commonly used testing method is pre-construction pile load testing, which can eliminate potential risks and uncertainties of piles subjected to various geotechnical conditions [18,28,4]. However, the pile load tests, which are usually performed on individual piles using frames and/or platforms in which dead loads are placed are costly and time-consuming and can be done on only a small number of piles on site.

In order to address some of these shortcomings, a relatively new method - thermal integrity profiling (TIP) has started to attract the attention of practitioners [1,30,6]. TIP captures temperature readings during the concrete curing process along the depth of the piles using

* Corresponding author.
E-mail address: ruiyi@tongji.edu.cn (Y. Rui).

https://doi.org/10.1016/j.engstruct.2022.114586
Received 18 February 2022; Received in revised form 17 May 2022; Accepted 25 June 2022
Available online 6 October 2022

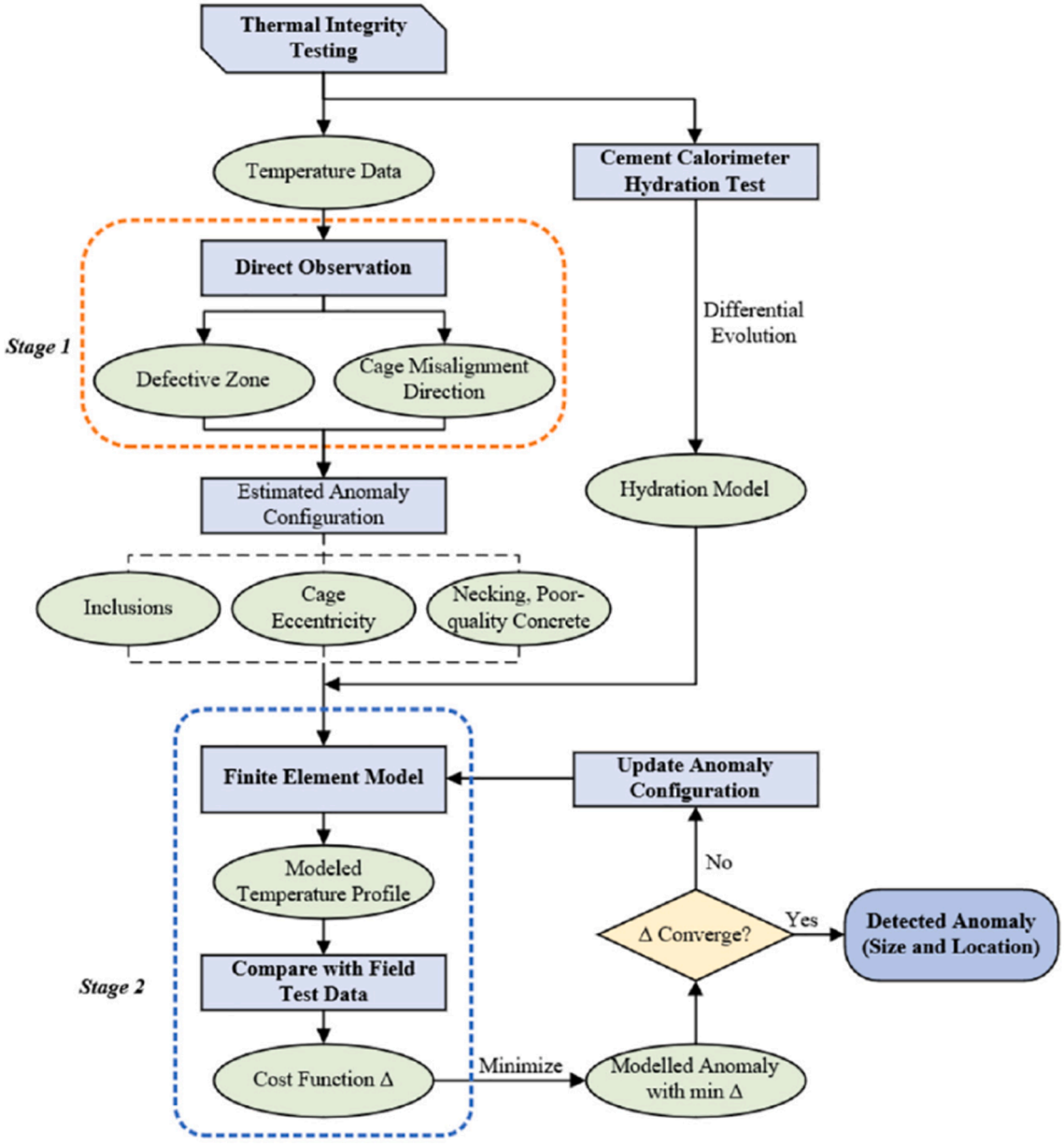

Fig. 1. Proposed framework for thermal integrity testing data interpretation - Sun et. al. (2020).

distributed or semi-distributed temperature sensors [25,27]. The temperature measurements are then compared against a theoretical model with the differences between the actual and the theoretical values attributed to anomalies inside the concrete [25,27]. Mullins & Johnson [23] undertook several experiments on piles with various built-in anomalies, which demonstrated the potential of the technique to locate different pile defects. Rui et al. (2018) used distributed fibre optic sensing technology to perform TIP testing and employed a one-dimensional numerical model to simulate the early age behaviour of a bored pile constructed in London. The article successfully assessed the integrity of the concrete cover, however, a key question, whether it is possible to identify anomalies within the concrete core (inside the steel cage), still remained. Recently, Sun et al. [31] proposed a framework which aims to facilitate the anomaly detection process for the cast in situ piles with higher accuracy. The basic elements of the proposed framework are shown in Fig. 1. The first stage includes direct observation of the temperature profiles to identify anomalous zones with the pile. This crucial stage, on which all subsequent analyses in the framework are built, is conducted manually and entirely relies on the judgement of the user. Hence, the initial identification of the potential problematic zones, relying on direct observation only, could be subjective and could lead to inconsistent outcomes for different users. The work presented in this paper addresses this specific key limitation and complements the work presented by Sun et al. [31].

The paper develops a novel anomaly detection approach combining the early-age concrete temperature monitoring data with finite element back-analyses. A CFA test pile with engineered inclusions (location, type and sizes are known in advance) was used to validate this method. The temperature data (along the entire depth of the pile) during the concrete curing process, complemented with a series of finite element back analyses facilitated the introduction of a key indicator, the effective pile radius, that could be reliably used to identify the locations of the engineered inclusions along the pile. This provides a consistent and reliable quantitative approach that replaces the direct observation proposed for Stage 1 of the thermal integrity testing data interpretation framework presented by Sun et al. [31]. The nature and size of these anomalies could be, qualitatively, inferred using the effective pile radius; however, this is more challenging and less reliable.

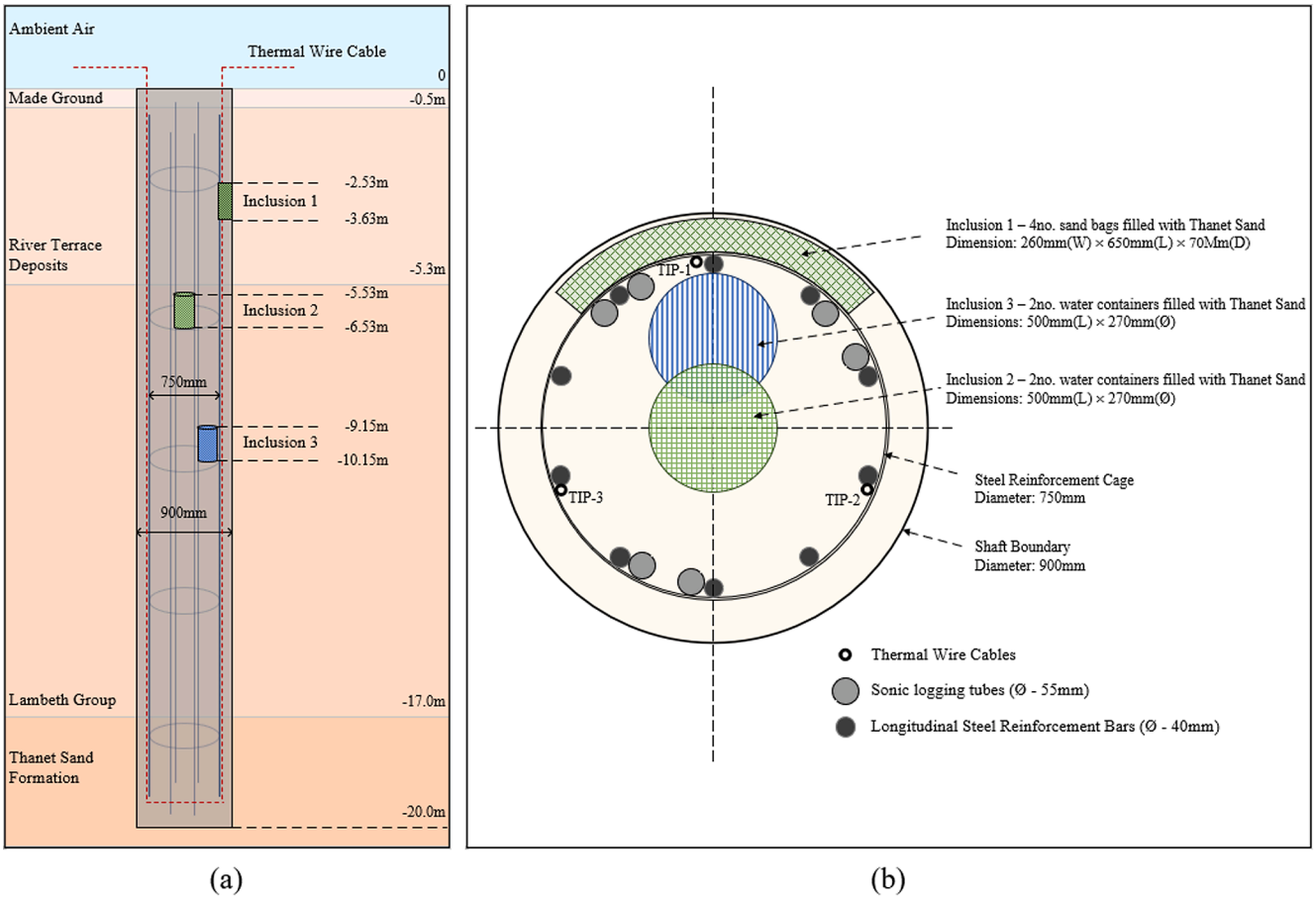

Fig. 2. (a) Soil stratigraphy and inclusion level; (b) pile instrumentation and reinforcement design.

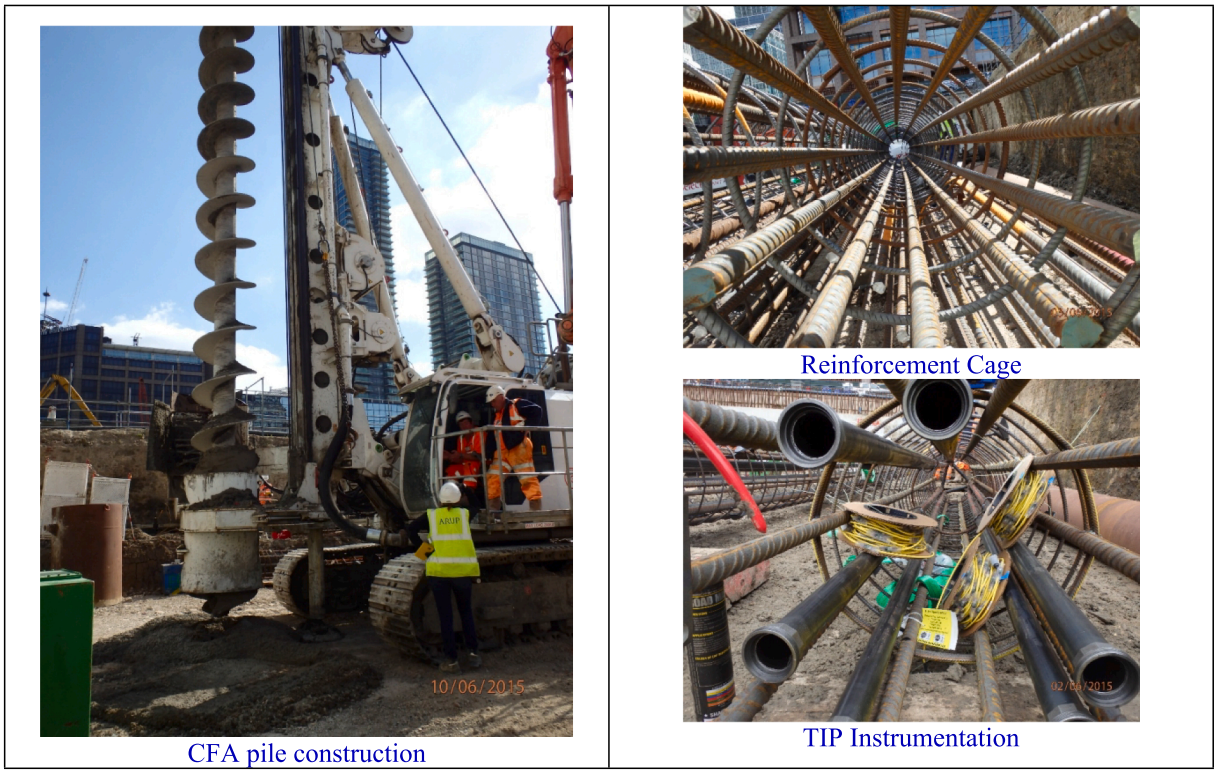

Fig. 3. Pile construction and TIP instrumentation.

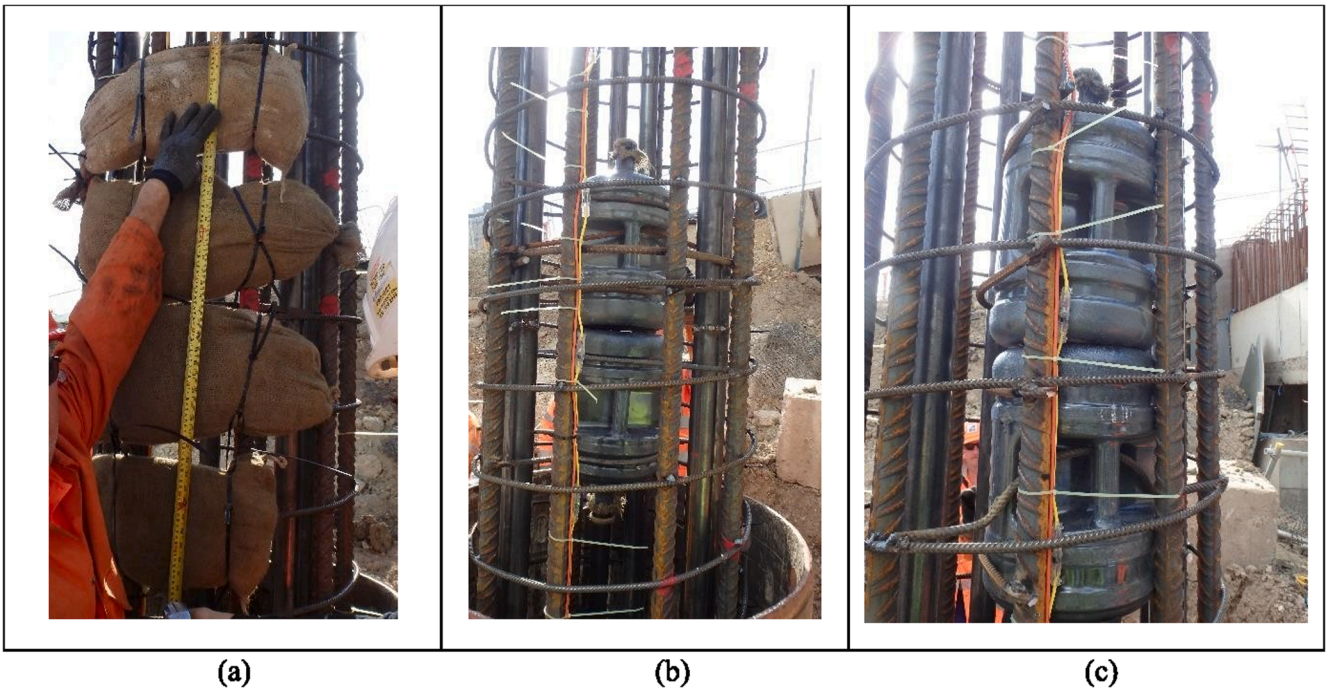

Fig. 4. Installation of inclusions positioned: (a) external to the cage; (b) centrally within the cage; (c) at the internal circumference of the cage.

2. Site instrumentation and temperature measurement

2.1. Test site and pile instrumentation

This project involved constructing and monitoring a continuous flight auger (CFA) test pile to enable a comparison between thermal integrity testing and the traditional cross-hole sonic logging. The test was conducted on 10 June 2015 in a construction site in London, United Kingdom. As shown in Fig. 2, the test pile had a nominal outer diameter of 900 mm and a designed length of 20 m. The reinforcement cage diameter was 750 mm and the temperature sensors for TIP were installed into the reinforcement cage before pile construction. The contractor records showed that a cumulative concrete volume of 15.28 m^3 was used to construct the pile. Site logs recorded that the soil excavation started at 16:59 pm and ended at 17:12 pm, followed by the concrete pouring (started at 17:12 pm and completed at 17:42 pm). Full-length TIP data collection was initialised at 17:15 pm - approximately 3 min after the start of concreting - and continued for 40 h which ended on June 12, 2015. The soil stratigraphy in the testing area consists of Made Ground, River Terrace Deposits which are underlain by the Lambeth Group and Thanet Sand formation as shown in Fig. 2(a). The TIP instrumentation included three thermal wire cables, namely TIP-1, TIP-2 and TIP-3 as shown in plan view in Fig. 2(b). A complete set of temperature measurements was collected every 15 min at 300 mm intervals along the pile length.

On the other hand, CSL was also conducted in this project to provide a comparison. Three cross-hole sonic logging tube pairs were attached to the reinforcement cage as shown in Fig. 2(b). After construction, probes (sensors that generate and detect signals) were lowered into the access tubes to conduct the CSL test. The transmitter probe sends a signal from one tube into the surrounding concrete, and the receiver measures the signal intensity on a different tube. The travel time between the tubes is then measured and is thus used as an indirect, low strain, non-destructive integrity test method that is most commonly used in deep foundations.

The test pile was constructed by rotating a continuous flight auger into the soil to build an empty shaft first. Upon reaching the design depth of 20 m, concrete was pumped through the hollow stem of the auger whilst the auger was slowly extracted (upwards). After the augers were withdrawn from the shaft, the reinforcement cage was plunged into the concrete that filled the shaft. As shown in Fig. 3, three thermal wire cables were attached on three sides of the reinforcement cage and routed along the full length of the pile.

Three engineered inclusions were constructed and attached to the cage at three different locations, as shown in Fig. 4, in order to assess the performance of TIP and CSL. Inclusion 1 is a set of sandbags filled with Thanet sand with a thickness of 70 mm installed externally to the reinforcement cage (Fig. 4(a)). This is used to simulate soil inclusions outside of the reinforcement cage, one of the most common forms of pile defects caused by limited collapse of shaft walls. Inclusions 2 and 3 are water containers filled with Thanet Sand. They were both 270 mm in diameter and placed in different locations along the pile (Fig. 4(b) and Fig. 4(c)). The soil inclusions within the reinforcement cage are represented by these two designed defects. It should also be mentioned that large holes or voids are also prevalent types of flaws that emerge during pile construction. Similar to soil inclusions, these defects do not generate heat. However, they have an even lower heat transfer rate, and thus have a greater impact on local temperature variation. As a result, large holes or voids are more noticeable in temperature profiles. For this reason, the field case study focuses on soil inclusions, a type of defect more difficult to detect by thermal integrity testing.

The spatial relation between the inclusions and the different sensors are shown schematically in Fig. 2 (a) and 1(b). The three inclusions were designed to be located at levels 2.53–3.63 m, 5.35–6.35 m and 9.15–10.15 m below ground level respectively. Inclusion 1 was close to TIP cable 1, located in the granular saturated River Terrace Deposits. Inclusion 2 was installed in the centre of the pile, while Inclusion 3 was installed at the cage's internal circumference, close to TIP cable 1.

2.2. Measured temperature profiles

Following the completion of the concrete pour, the three thermal wire cables generated a set of temperature measurements every 15 min at 300 mm intervals along the cables. Hence, there are three independent temperature/time readings for each cross-section at 300 m intervals along shaft length. The end of the concrete pour is designated as

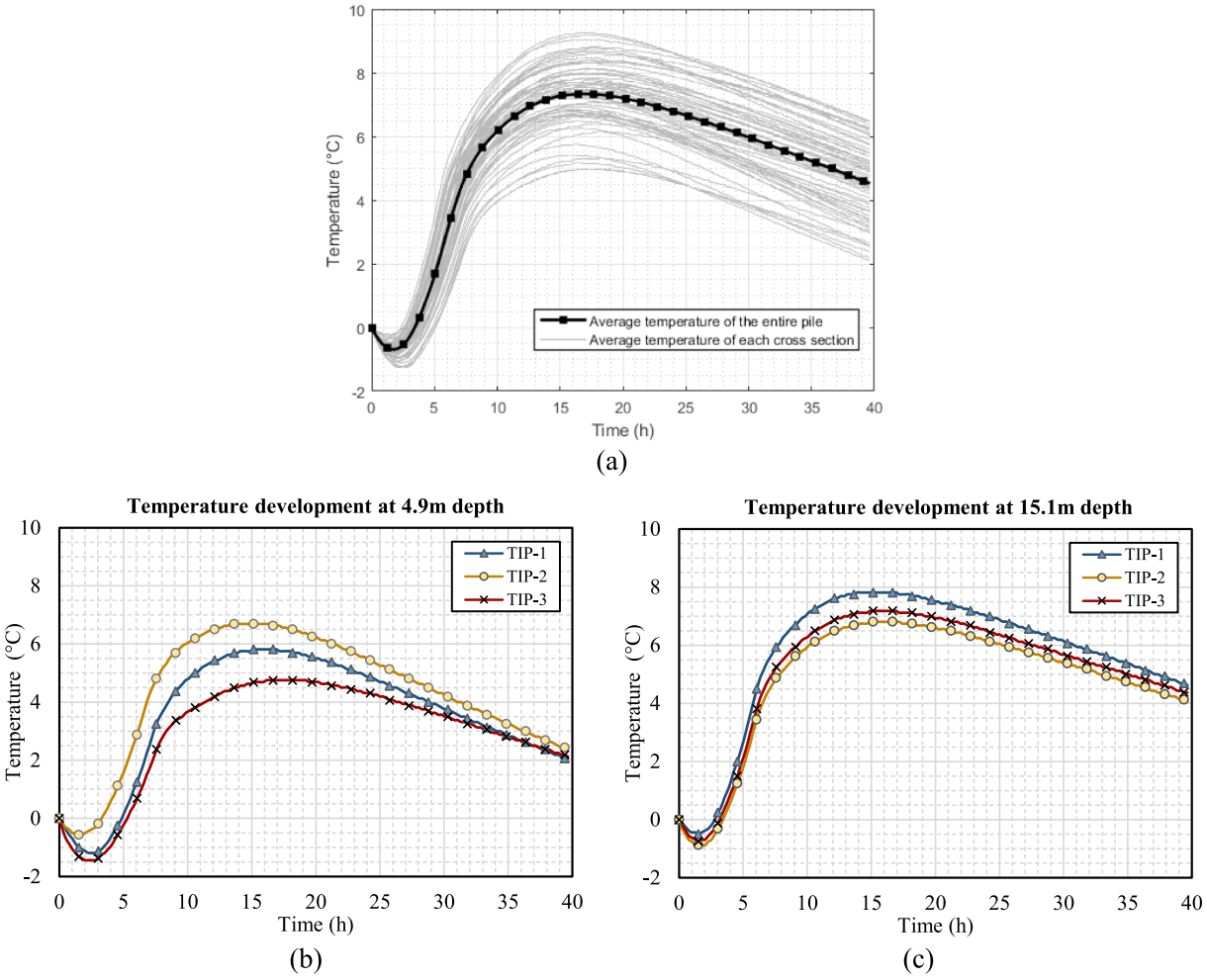

Fig. 5. Thermal wire cable temperature development over time.

the baseline from which curing time is measured. The average values of the three temperature measurements in each cross-section over 40 h monitoring period are plotted using the light grey lines shown in Fig. 5 (a). The black line represents the mean value of all the sensor measurements. The observed trend shows a small decrease in temperature over the first 2 h followed by a steep increase in the temperature over the next 20 h, after which the rate of heating started to drop. The maximum temperature is observed between 14 and 16 h from the initial reading, about 7 °C warmer than the initial value. The different peak temperatures between the cables show that the pile did not see a uniform maximum temperature on each cross-section. The difference ranged from 5 to 8 °C despite a similar heating rate across the cables. Steady cooling started after the peak, with the temperature gradually reducing for the remainder of the test. For a pile without any defects, the peak temperature at different cross-sections should be reasonably uniform along the entire depth. Hence, these different peak temperatures in Fig. 5 (a) indicate non-uniform properties for the pile. Some of these non-uniform properties were due to the defects in the pile. Fig. 5 (b) and (c) show the temperature change for the three separated temperature cables on two cross sections at 4.9 m and 15.1 m deep over a 40-hour monitoring period. TIP-1, which is close to Inclusion 1 at 4.9 m, has a substantially lower temperature than TIP-2 in Fig. 5 (b). Lower TIP-3 temperature may result from misaligned reinforcement cages or necking issues at this depth. In contrast, the temperature on all three cables at 15.1 m in Fig. 5 (c), which is far from any design inclusions, is relatively similar.

In addition to temperature development at specific measurement points, the longitudinal temperature profiles along thermal wire cables also contribute significantly to pile integrity assessment. As the concrete hydration process is time-dependent, the optimum time to conduct the profile analysis is crucial for distinguishing regions of suspected anomalies within the piles. The ASTM Standard [2] suggest that the optimal testing time should be “near the time of peak temperature in the concrete” when “the maximum contrast to the surrounding material” occurs, which, according to Fig. 5, is around 15–16 h after concrete casting in this case study. On the contrary, recent studies [30,6] suggest the greatest thermal effect due to defects occurs at the time of the maximum rate of temperature rise, which is 6 h after concreting in this case study. Thus, two sets of temperature profiles corresponding to the highest temperature rise rate and the peak temperature are plotted in Fig. 6. The designed locations of the three engineered inclusions and the ground soil layers are illustrated in the figure by shaded boxes and various background colours respectively. Using visual inspection, both Fig. 6 (a) and (b) show significant temperature reductions at 2.5 m, 6.5 m and 9.5 m, all of which are near the designed locations of engineered inclusions.

3. Developing the new anomaly detection approach

3.1. Pile general temperature profiles

The temperature development of a cast-in-situ pile depends on many factors, including concrete mix, cement type, shaft size and boundary conditions. The cement composition and concrete mix determine the hydration model, and thus define the heat generation rate of the early

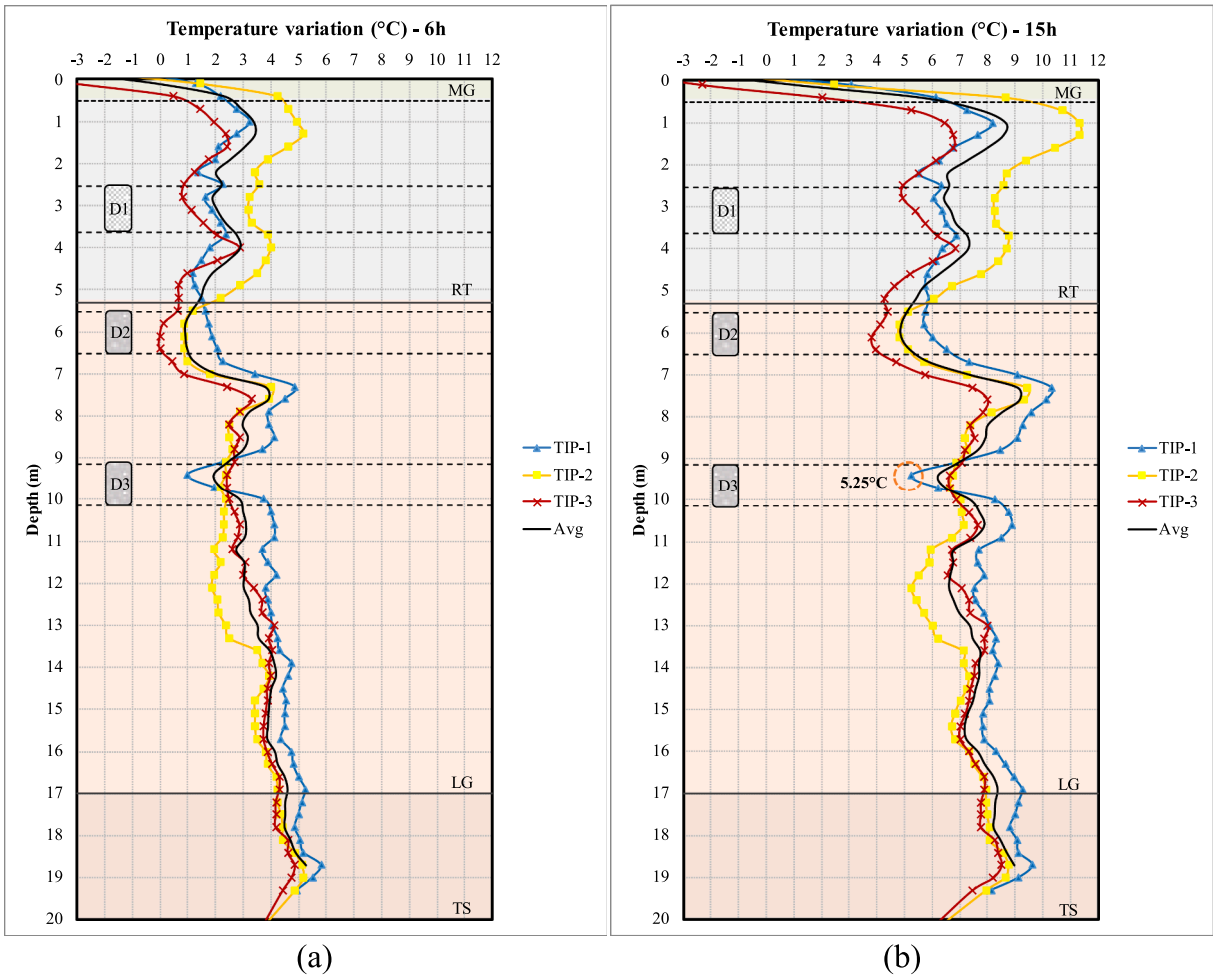

Fig. 6. Longitudinal temperature profiles at (a) 6 h and (b) 15 h after concrete casting.

age concrete. The shaft geometry and boundary determine the heat transfer route and speed. The heat dissipation and temperature distribution for an idealised cast-in-situ pile are illustrated schematically in Fig. 7. For a cylindrical pile without defects, the cross-sectional lateral temperature distribution is bell-shaped with the peak at the shaft centre. The soil with higher thermal conductivity allows faster heat transfer from the concrete body to the surrounding soil, leading to lower central temperature. The larger shaft size increases the amount of heat source and the route of heat dissipation, thus higher central temperature would be expected to occur. If the soil thermal conductivity changes between the different soil layers, the various heat dissipation rates lead to vertical temperature profile variation. Generally, a significant temperature "roll-off" exists on the top and bottom of the vertical profile, which can be seen on the measured temperature profiles in Fig. 6. The bottom of the shaft allows heat dissipation not only radially out of the circumference but also longitudinally through the end. The top of the shaft is exposed to the ambient environment (air), and hence internal heat is dissipated much faster than other locations. Thus, the temperature is usually several degrees Celsius lower than the average profile temperature in the upper and lower one–diameter length of the pile.

In practice, anomalies such as voids, necking, bulging and soil intrusion may exist inside the concrete body of the piles mainly due to construction related factors (including but not limited to shaft condition, open time of the shaft before concreting, shaft excavation techniques, etc…). O'Neil and Sarhan [26] reported that more over 20 % of 2986 drilled shaft piles evaluated in California between 1996 and 2000 had serious defects that could compromise pile loading capacity. Jones and Wu [16] and Camp et al. [9] investigated cross-hole sonic logging on 1000 and 441 drilled shafts, respectively, in the United States under diverse ground conditions. The findings show that between 33 % and 38 % of these piles had at least one structural defect. Fig. 8 shows examples of drilled shaft pile defects. Fig. 8 (a) illustrates severe concrete material loss near the surface, while Fig. 8 (b) displays a soldier pile wall with multiple defects such as necking, void, and misaligned reinforcement cage.

The measured temperature at the sensor location is affected by multiple factors, including shaft size, boundary condition and presence of any anomalies. It is usually difficult to distinguish one factor from another. Specifically, the temperature measurement of an anticipated intact concrete pile could be similar to a defective concrete pile with a larger radius. Fig. 9 shows an example of such a scenario where the recorded temperature at S1 in the first pile is close to the temperature at S2 in the second pile near the defect. Therefore, in this paper, to address this specific situation, temperature profile variation in each soil layer will be considered as a change in the 'effective pile radius', which denotes the radius of an intact pile that produces a similar amount of heat and generate the same measured temperature at the sensor location. Thus, the value of the effective pile radius (R_{eff-S1}) at S1 location should be close to that (R_{eff-S2}) at S2 location shown in red dashed line in Fig. 9. The effective pile radius along the entire shaft is a crucial indicator for pile quality assurance. Engineers can use effective pile radius to make a quick assessment whether detailed integrity investigations are required for the pile in question or not. Given that the temperature sensors are attached to the reinforcement cage with a known radius, the effective pile radius (R_{eff}) can also be related to the effective pile cover thickness (D_{cover}) using the following equation:

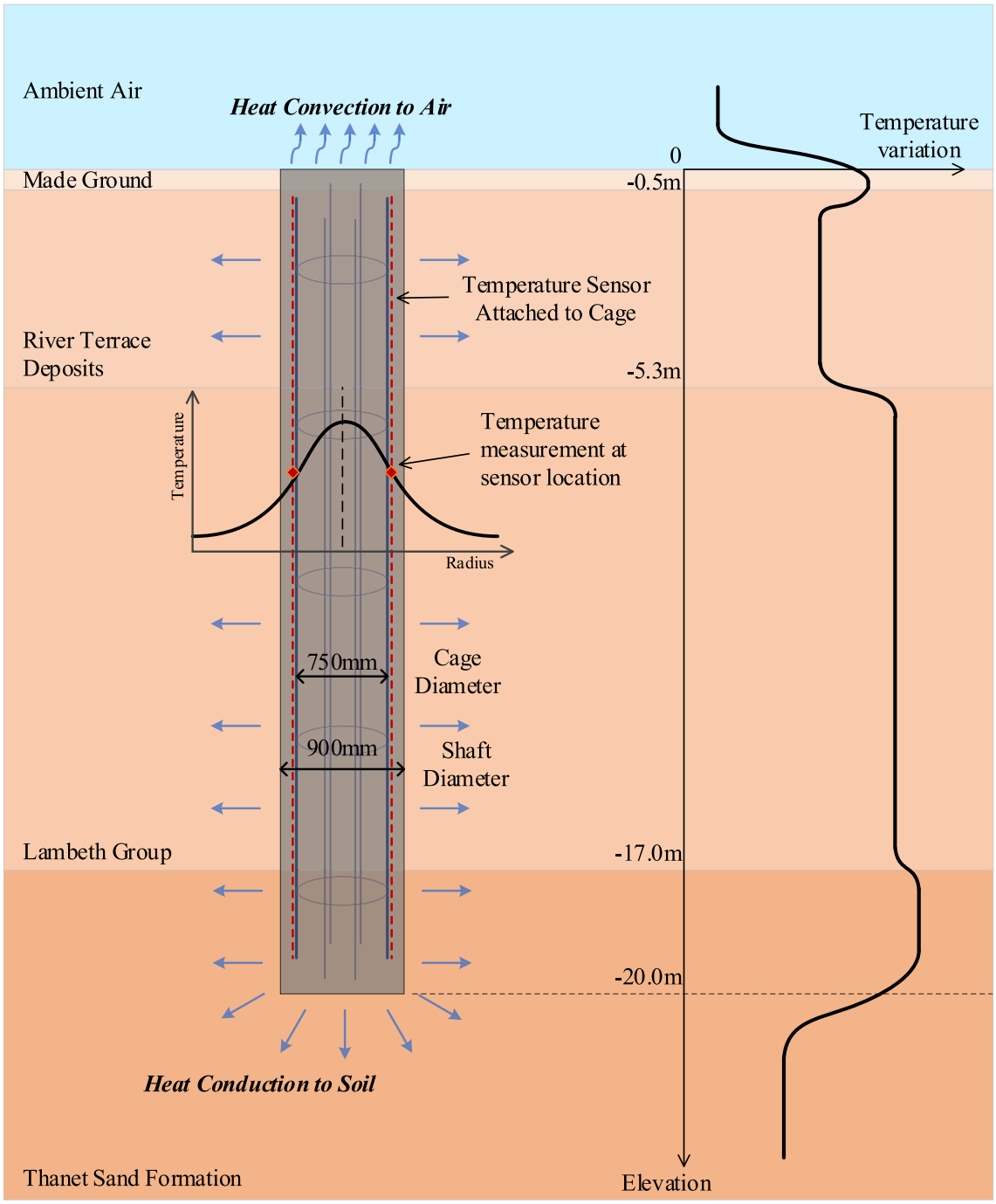

Fig. 7. Temperature profile for a perfect cylindrical pile without defect.

$$R_{eff} = r_{cage} + D_{cover} \quad (2)$$

where r_{cage} is the radius of the reinforcement cage.

3.2. Finite element and hydration model

All the changes in temperature profiles (along the depth of the pile) are assumed to be due to the variation in effective pile radius. These temperature profiles can also be computed using one-dimensional (1D) finite element analyses (in three radial directions corresponding to the three sensor locations within the pile) of heat transfer in which effective pile radii are assumed along the pile depth. The effective pile radius is adjusted at different locations along the pile depth to get a good match between the measured temperature profile and that calculated by the FE analyses. Through this method, the effective radius along the depth of the pile can be predicted in three sensor radial directions corresponding to the three sensors arrays. After analysing all cross-sections, the geometry of the whole test pile can then be computed. Due to the axial symmetry, the finite element model can be simplified as a 1D model, as shown in Fig. 10. The FE model includes pile elements and soil elements; the hydration heat source is applied to every node of the pile elements to simulate the hydration heat production. The pile/soil interface location (or concrete cover thickness) is adjusted in the FE analysis to match the predicted temperature with the monitoring data.

The accuracy of the hydration model will directly affect the finite element temperature prediction and the anomaly detection capability.

Fig. 8. (a) A drilled shaft with severe necking; (b) a soldier pile wall with numerous defects [24].

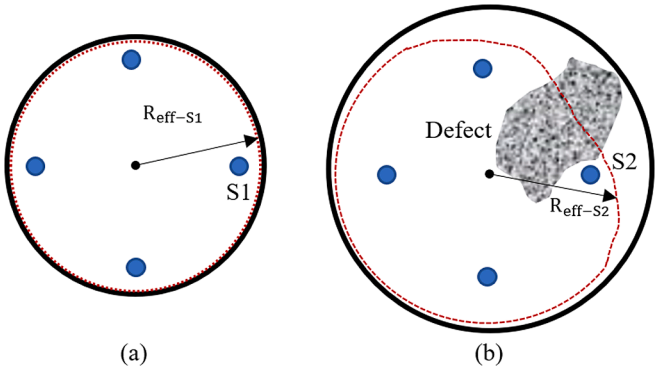

Fig. 9. (a) A smaller pile without defect, (b) a larger pile with defect.

Many formulations have been developed over the years to quantify hydration heat production. The work presented in this paper employes the hydration model proposed by De-Schutter and Taerwe [11,12]. The model has explicit and relatively simple mathematical expressions. The heat production rate of concrete $Q\,(J/gh)$ is expressed as a function of the actual temperature and the degree of hydration:

$$Q = cw \cdot q_{max,20} \cdot c \cdot [sin(\alpha_t \pi)]^a \cdot e^{-b\alpha_t} \cdot e^{\frac{E}{R}\left(\frac{1}{293}-\frac{1}{T}\right)} \tag{3}$$

where a, b and c are hydration parameters dependent on material properties; α_t is the degree of hydration, defined as the proportion of the amount of heat released at time t to total heat of hydration Q_{total}; $q_{max,20}$ is the maximum heat generate rate at 20°C; E is the apparent activation energy; R is the universal gas constant; T is the temperature of concrete (K); and cw is the percentage of cementitious materials by weight. Table 1 shows the Type I cement hydration parameters obtained from experimental data by De Schutter & Taerwe [11]. It should be noted here

Table 1
Calibrated hydration model parameters.

Parameters	a	b	c	E kJ/mol	$q_{max,20}$ J/gh	Q_{total} J/g
De Schutter [11]	0.667	3.0	2.6	33.5	7.79	270
Sun et al. [31]	0.787	3.3	3.0	28.0	9.91	161

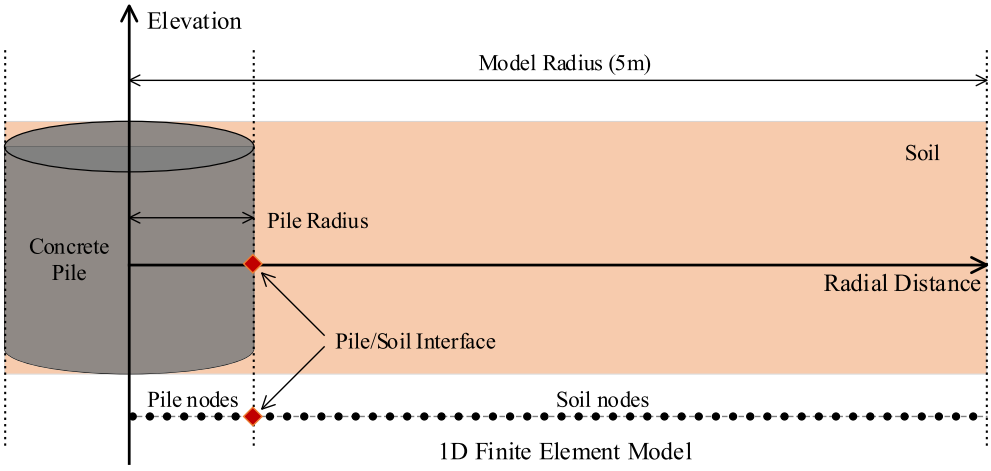

Fig. 10. 1D axisymmetric heat transfer finite element model.

Table 2
Concrete mix design.

Material	Type	Source	Weight SSD* (kg/m^3)	Proportion constituent	Proportion by total weight
Cement	CEM I	Ketton	190	50 %	8.0 %
	GGBS	Purfleet	190	50 %	8.0 %
Limestone Aggregates	10–20 mm	Whatley	520	29 %	21.8 %
	4–10 mm	Whatley	420	23 %	17.6 %
	0–4 mm	Greenwish	870	48 %	36.5 %
Admixture	Limestone filler	Omya	40	–	1.8 %
	Viscoflow 2000*	Sika	2.52	–	0.1 %
Water	–	Network Water	152	–	6.4 %
Total Weight			2385	–	–

SSD*: Saturated surface dry (SSD) defined as the condition of an aggregate in which the surfaces of the particles are "dry" (i.e., surface adsorption would no longer take place), but the inter-particle voids are saturated with water.
ViscoFlow 2000*: A liquid admixture for concrete based on unique polycarboxylate polymers technologies. ViscoFlow 2000 is designed as a high range water reducer or superplasticiser. It is particularly suited for use in concretes that require low water/cement ratios and / or high water reductions with excellent workability retention properties of up to 3 h [https://sikaconcrete.co.uk/products-systems/sika-viscoflow-2000/].

Table 3
Values of thermal properties.

Parameters	Top of Strata (m)	Thermal conductivity k (W/mK)	Volumetric heat capacity ρc(KJ/m^3K)	Thermal diffusivity K (10^{-6} m^2/s)
Made Ground	0.0	1.8	2800	0.64
River Terrace Deposits	0.5	2.0	2000	1.00
Lambeth Group	5.3	1.6	2200	0.73
Thanet Sand Formation	17.0	1.6	2400	0.67
Chalk	31.4	1.4	2400	0.58
Concrete Pile	–	1.1	2300	0.48

that the values of these hydration material parameters vary considerably for different concrete mixtures and cement composition.

The test CFA pile also employed Type I cement but with a different composition and mix design. The cement proportion *cw* can be determined from concrete mix design in Table 2, where cementitious materials account for 16 % of total weight. The hydration material parameters for this field test are calibrated using the field-testing data and differential evolution algorithms as detailed in Sun et al. [31]. The results are listed in Table 1. The significant difference between the two sets of parameters is the value of Q_{total}. The calibrated value of Q_{total} is about two thirds of that obtained from experimental data by De Schutter; this is possible because half of the cementitious material has been replaced by ground granulated blast-furnace slag (GGBS) in this field case study.

The initial temperature of the soil was fixed at an assumed ground temperature of 13 °C [13,31]. The initial temperature of concrete at casting ranged from 22−24 °C obtained from the temperature sensor measurement. The soil thermal properties in this field test also vary in different soil strata as listed in Table 3 (average values were selected from a number of studies including Rui et al. [29], Garber [13] and Kim et al. [17]. In the pile construction log, the actual pile length recorded was 20.02 m, with a total concrete consumption of 15.28 m^3. The designed diameters of shaft and reinforcement steel cage were 900 mm and 750 mm, respectively, as illustrated in Fig. 7. As temperature sensors were attached to the cage, the sensor radial position to the shaft centre was 375 mm.

3.3. Data analysis and interpretation

Relationship between maximum temperature and effective radius.

In the thermal integrity test, the temperature sensor cables are attached to the outer layer of the reinforcement cage. As the temperature at the pile centre and concrete cover is unknown, the measured

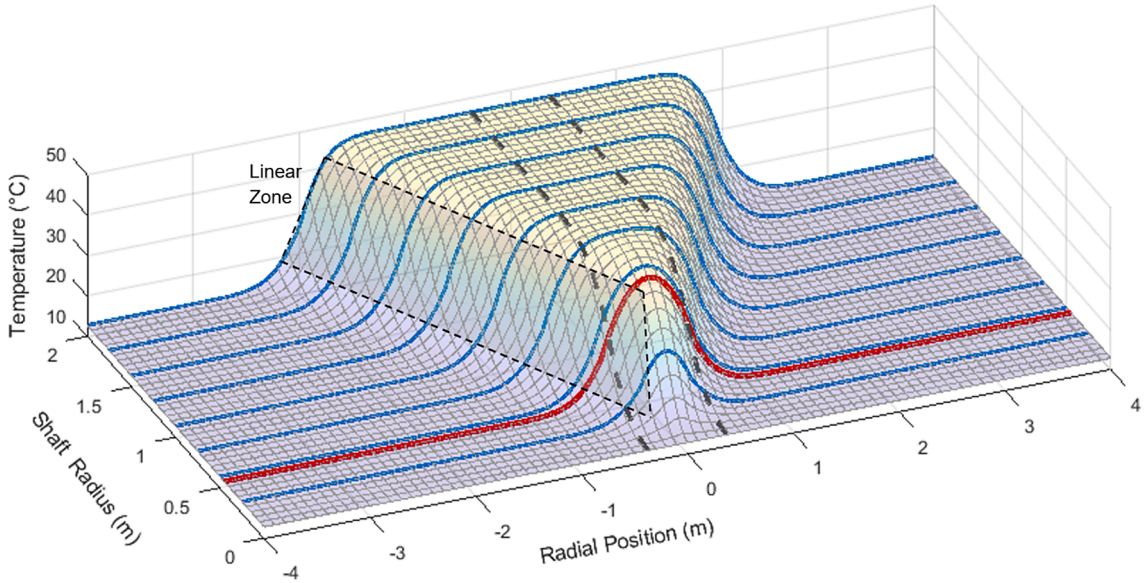

Fig. 11. Relationship between cage position, shaft size and temperature measurement at 16 h.

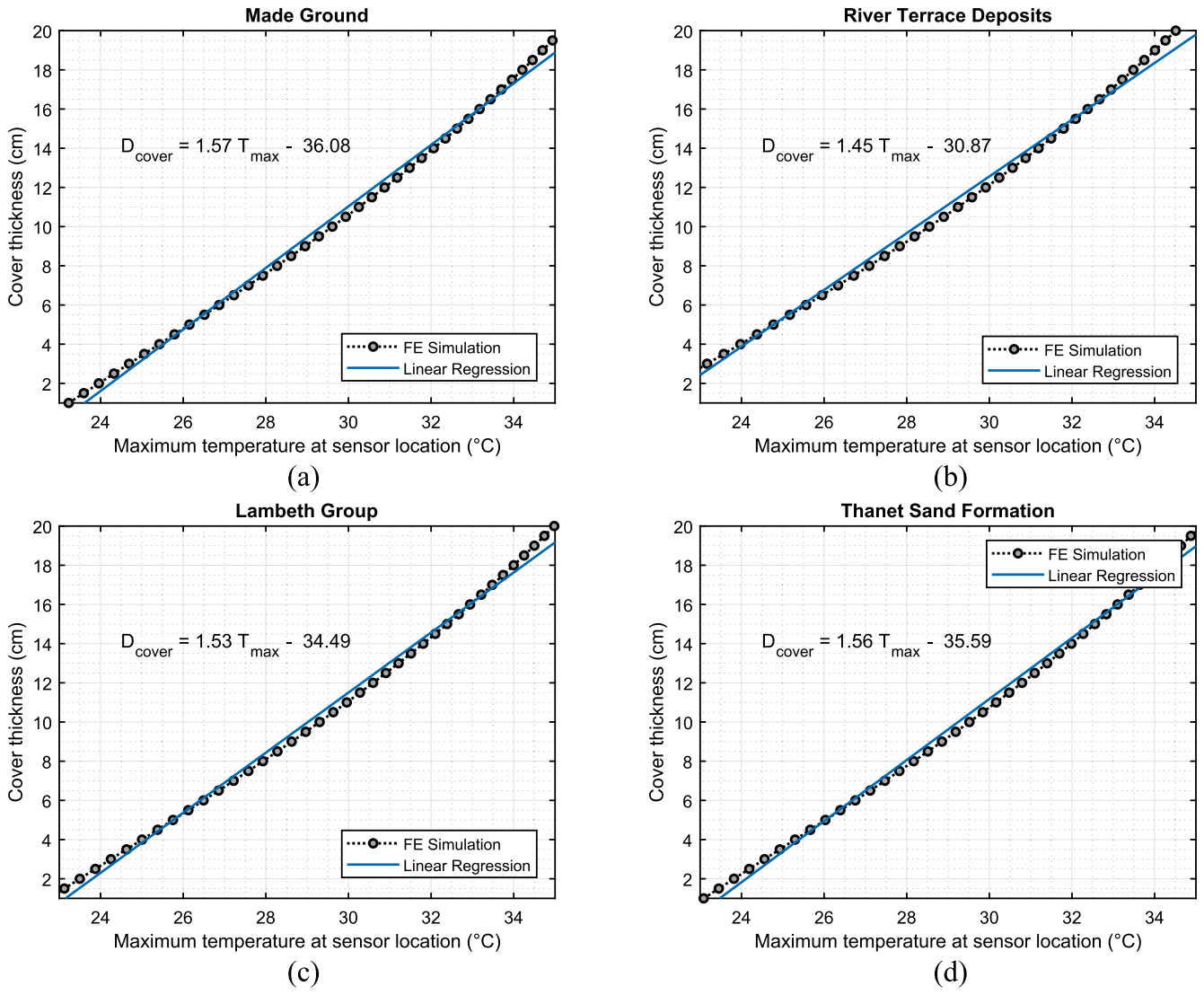

Fig. 12. Linear relationship between concrete cover thickness and maximum temperature.

temperature data at the cage location are used to infer the entire pile temperature distribution and predict potential defects. Therefore, the relationship between temperature measurement and shaft size for an intact concrete pile needs to be investigated. Fig. 11 shows a theoretical relationship (using the hydration model proposed by De-Schutter and Taerwe [11,12] with the parameters presented in the tables above) for cage radius, shaft radius and temperature at 16 h after the concrete pour (time to peak temperature). The thick dashed lines represent the cage position where temperature sensors are attached, and it is 0.375 m in this field case study. The solid lines represent different shaft radii - the red line represents a shaft radius of 0.45 m as in the field test. The solid and dashed lines intersect at the theoretical temperature measurement. The predicted peak temperature (in the middle between the dashed lines) increases linearly with the increase of shaft radius. As the common design for pile concrete cover is usually between 25 mm and 200 mm thick, the shaft size and temperature still fall into the linear relationship zone in Fig. 11 [22]. Therefore, the temperature measurement at the cage location is highly sensitive to the concrete cover thickness, which can be a good indicator to assess the as-built pile shape.

The method suggested by Mullins [22] requires the practitioner to select a temperature distribution profile at a specific time. For example, Johnson [15] employed temperature measurement 24 h after concrete casting. However, it is not easy to determine the most appropriate time as relationship between cage position and shaft size (as shown in Fig. 11) changes at different temperature measurement time – please note that Fig. 11 is plotted at 16 h following concrete casting. It is even more challenging to conduct pile shape analysis with a time-dependent temperature-radius relation. To generalise the proposed method, this study employs the maximum temperature at each measurement point within the entire curing period instead of the temperature distribution at a specific time. The maximum temperature at each sensor location is also strongly related to pile shape, concrete quality and boundary conditions, and it can be easily extracted from the measurement data. It is expected that a similar linear relationship between maximum temperature and shaft radius should be found through 1D FE analysis.

A series of 1D finite element models (as detailed in Section 3.1) were established in four layers of soil; Made Ground, River Terrace Deposits, Lambeth Group and Thanet Sand Formation, where the main body of the pile was located. In each soil layer, a number of FE simulations were conducted using different concrete cover thickness in each simulation. The thickness ranged from 1 cm to 20 cm with an interval of 0.5 cm. All other parameters, including reinforcement cage location, concrete and soil thermal properties, follow the pile design and construction specifications.

The maximum temperature at the sensor location (as specified in the field test – 375 mm from the centre of the pile) corresponding to each

Table 4
Values of D-T relationship parameters.

Parameters	α_k(cm/°C)	β_k(cm)
Made Ground	1.57	36.08
River Terrace Deposits	1.45	30.87
Lambeth Group	1.53	34.49
Thanet Sand Formation	1.56	35.59

Table 5
Changes in $\boldsymbol{\alpha_k}$ with variation of thermal diffusivity of soil and temperature sensor location.

α_k(cm/°C)		Sensor Location (m)					
		0.35	0.36	0.37	0.38	0.39	0.40
$\mathbf{K_{soil}}$ $(\mathbf{k}/\boldsymbol{\rho}.\mathbf{c})(m^2/s)$	0.4	1.79	1.76	1.73	1.71	1.68	1.67
	0.5	1.70	1.67	1.64	1.62	1.60	1.60
	0.6	1.64	1.61	1.58	1.56	1.54	1.54
	0.7	1.59	1.56	1.53	1.51	1.50	1.50
	0.8	1.56	1.52	1.49	1.47	1.46	1.46
	0.9	1.53	1.49	1.46	1.44	1.43	1.43
	1.0	1.50	1.46	1.43	1.41	1.40	1.41
	1.1	1.48	1.44	1.41	1.39	1.38	1.39
	1.2	1.46	1.42	1.39	1.37	1.36	1.37

different concrete cover thickness is extracted and illustrated in Fig. 12. A strongly linear relationship between maximum temperature and cover thickness is revealed for the different soils boundary conditions as follows:

$$D_{cover} = \alpha_k * T_{max} - \beta_k \quad (4)$$

where D_{cover} represents the concrete cover thickness (cm) and T_{max} denotes the maximum temperature (°C) at the measurement point, α_k (cm/°C) and β_k (cm) are D-T parameters dependent on factors including sensor location and soil material. The value of these parameters were obtained through linear regression of the FE analysis data and are listed in Table 4. For example, in the Lambeth Group, the parameter α_k implies that every 1 °C increment of the measured maximum temperature represents 1.53 cm increase of the concrete cover thickness, which provide a convenient approach to evaluate pile effective radius.

Parametric study of soil thermal property and sensor location.

The thermal properties of soil vary among different strata, and hence it is necessary to evaluate its impact on D_{cover} - T_{max} relationship. Meanwhile, due to the cage misalignment or sensor attachment error on the steel reinforcement bar, temperature sensors may not precisely be located at their specified locations (375 mm away from the centre of the pile cross-section in this case). Thus, a series of parametric studies were performed to investigate the effect of soil thermal properties and sensor locations on the parameters α_k and β_k.

The heat dissipation rate in soil does not solely depend on soil thermal conductivity k (W/m.K), but is also affected by soil density ρ (kg/m^3) and specific heat capacity c (J/kg.K). Thus, a collective factor, the thermal diffusivity K_{soil} is used for this parametric study, defined as:

$$K_{soil} = k/(\rho.c) \quad (5)$$

The reference value of K_{soil} for the soil in Lambeth Group is 0.73 m^2/s (from Table 3), and the reference sensor location is 0.375 m as mentioned previously. A series of one-dimensional FE models simulations were conducted for K_{soil} ranging from 0.4–1.2 m^2/s and sensor location varying from 0.35 to 0.40 m. All the analyses results for α_k and β_k are listed in Table 5 and Table 6. The value of α_k remains between 1.37 and 1.79 cm/°C and is inversely proportional to the values of thermal diffusivity K_{soil} and sensor location.

It is worth noting here that the D-T relationship parameters α_k and β_k also depend on serval other factors, such as seasonal ground temperature variation and concrete thermal conductivity.

3.4. Pile 3D shape analysis

The relationship between the maximum temperature and concrete cover thickness allows us to back-calculate the temperature development at three different sensor locations on the cross-sections along the pile depth spaced at 300 mm. This back-calculation aims to obtain the effective pile radius along the pile using Eqs. (2) and (4). Four sets of D-T relationship parameters α_k and β_k are applied for four different soil layers (Made Ground, River Terrance Deposits, Lambeth Group and Thanet Sand). The calculated pile effective radius in the three different axial directions (sensor locations) are shown in Fig. 13. The results show noticeable radius variation along the shaft. Between 2 and 4 m, the effective radius at the location of TIP-2 sensor is significantly larger than that at the location of TIP-3 sensor by around 7 cm. At TIP-1 location, a sharp decrease of the effective radius can be seen between 8 and 9 m below ground, and the radius is larger than average along the bottom half part of the pile.

The results obtained above are then used for constructing the pile 3D shape. The radius values at the three axial directions along the depth of the pile are first calculated by spline interpolation (longitudinally). It is a form of interpolation method which use a special type of piecewise polynomial called a spline [5,20,21]. The spline interpolation offers better continuity between the segments compared to linear interpolation. Then the effective radius on each cross-section is again calculated by spline interpolation based on the values at the three sensor locations (spline interpolation now applied in each cross-section). On each cross-section, only three data points are available, and this could result in interpolation discontinuity. Thus, the known radius values are repeated on the X-axis from 0 to 6 π with each interval of a full circle 2 π as shown in Fig. 14. A continuous profile of the effective radius between 2 π and 4 π is extracted as the final prediction. Using Fig. 14 ensures that the slope at 2 π and 4 π is the same as they are on the same radian location on the pile cross-section. For a given cross-section, the result of this analysis provides predicted effective radius values which enables the shape of the cross-section to be determined. The above procedure is then repeated for all the cross-sections spaced at 300 mm along the pile and eventually a

Table 6
Changes in $\boldsymbol{\beta_k}$ with variation of thermal diffusivity of soil and temperature sensor location.

β_k(cm)		Sensor Location (m)					
		0.35	0.36	0.37	0.38	0.39	0.40
$\mathbf{K_{soil}}$ $(\mathbf{k}/\boldsymbol{\rho}.\mathbf{c})$ $(\mathbf{m^2/s})$	0.4	−46.11	−44.28	−42.61	−41.06	−39.60	−38.27
	0.5	−42.45	−40.58	−38.88	−37.37	−36.09	−35.03
	0.6	−39.79	−37.90	−36.18	−34.69	−33.50	−32.59
	0.7	−37.75	−35.85	−34.12	−32.63	−31.50	−30.68
	0.8	−36.14	−34.23	−32.47	−30.99	−29.90	−29.14
	0.9	−34.82	−32.90	−31.13	−29.64	−28.58	−27.86
	1.0	−33.71	−31.78	−30.01	−28.52	−27.47	−26.78
	1.1	−32.77	−30.84	−29.05	−27.56	−26.52	−25.85
	1.2	−31.96	−30.02	−28.23	−26.73	−25.71	−25.04

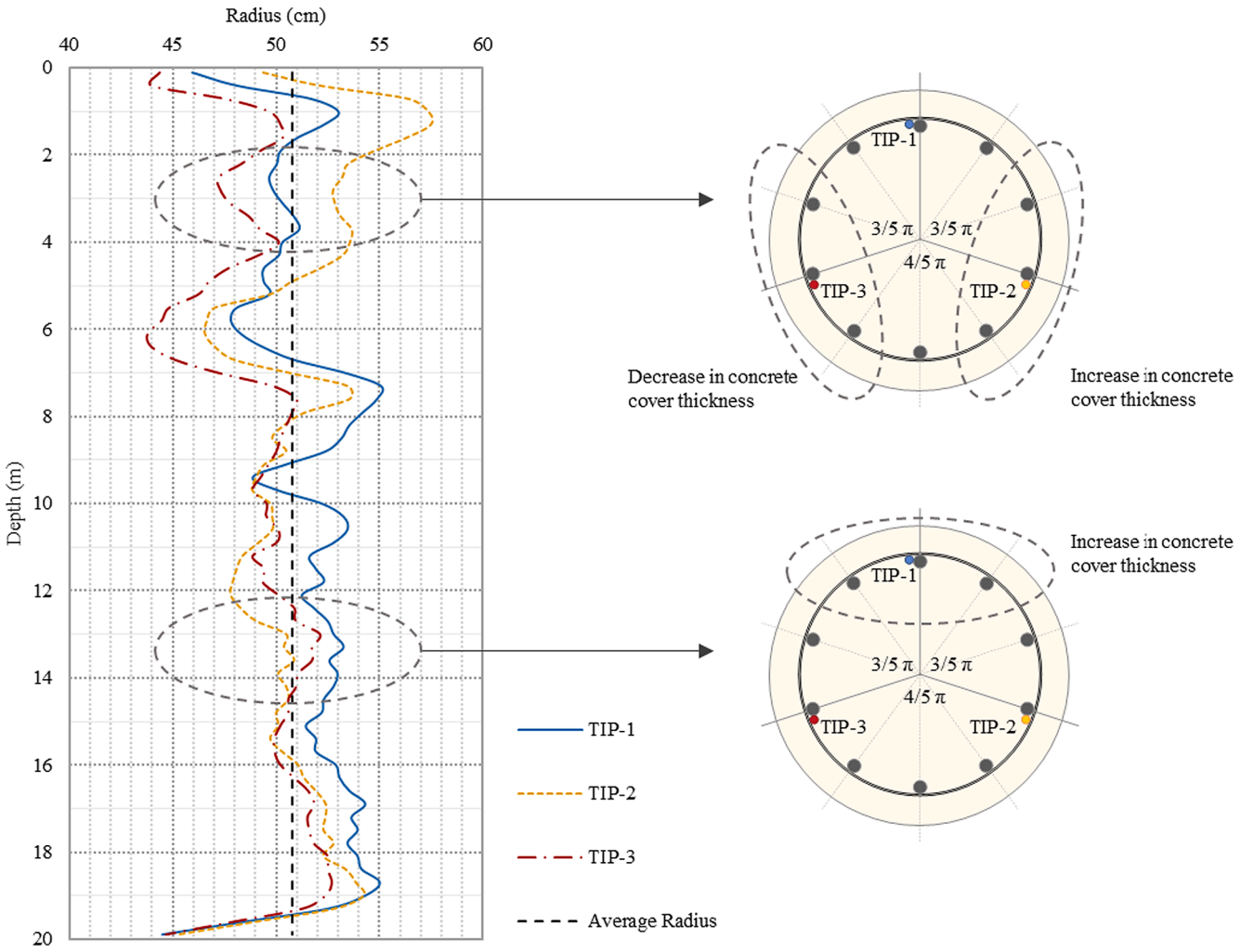

Fig. 13. Pile effective radius in three axial directions along the pile length.

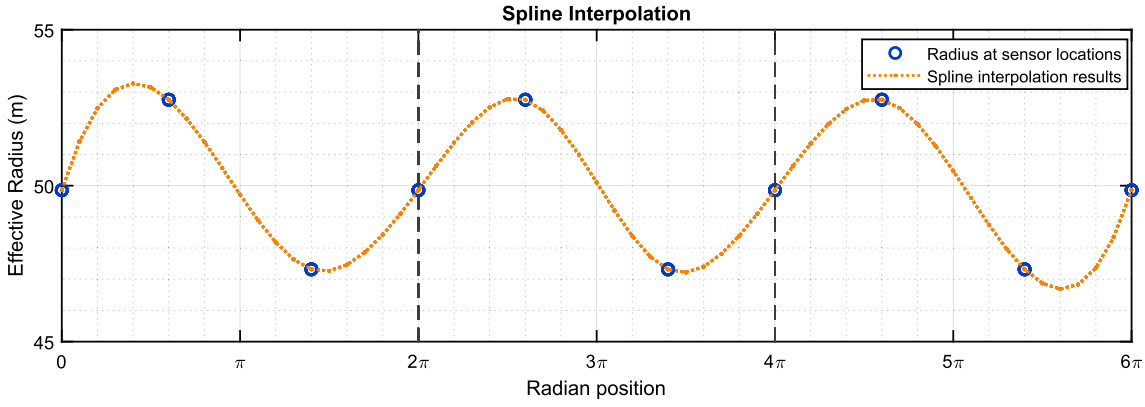

Fig. 14. Spline interpolation of pile effective radius at 2.8 m depth.

continues 3D pile shape is obtained. The key advantage of using this method is that the presence of any anomaly, whether located within the steel cage or outside, will affect the shape of the cross-section as long as the anomaly is significant enough to affect one or more of the sensor readings.

Fig. 15 shows the 3D pile shape according to the calculated effective radius. The average pile effective radius is around 50.7 cm (this is calculated by getting the average effective radius for every cross-section and then averaging over the whole length of the pile). The absolute largest (bright yellow in Fig. 15 and absolute smallest (dark blue in Fig. 15) radii are 57.5 cm and 43.5 cm, respectively. The orange colour indicates an expanded pile radius over the average value 50.7 cm, and blue colour represents a contracted pile radius smaller than the average value which are marked as defective zones. Two minor defective zones can be seen in Fig. 15 between 2 and 4 m and 9 to 12 m below the ground appears, and one severe defective zone shown as dark blue area between 6 and 8 m appears to be a significant necking problem. The pile radius varies significantly along the upper half part of the pile, where it ranges

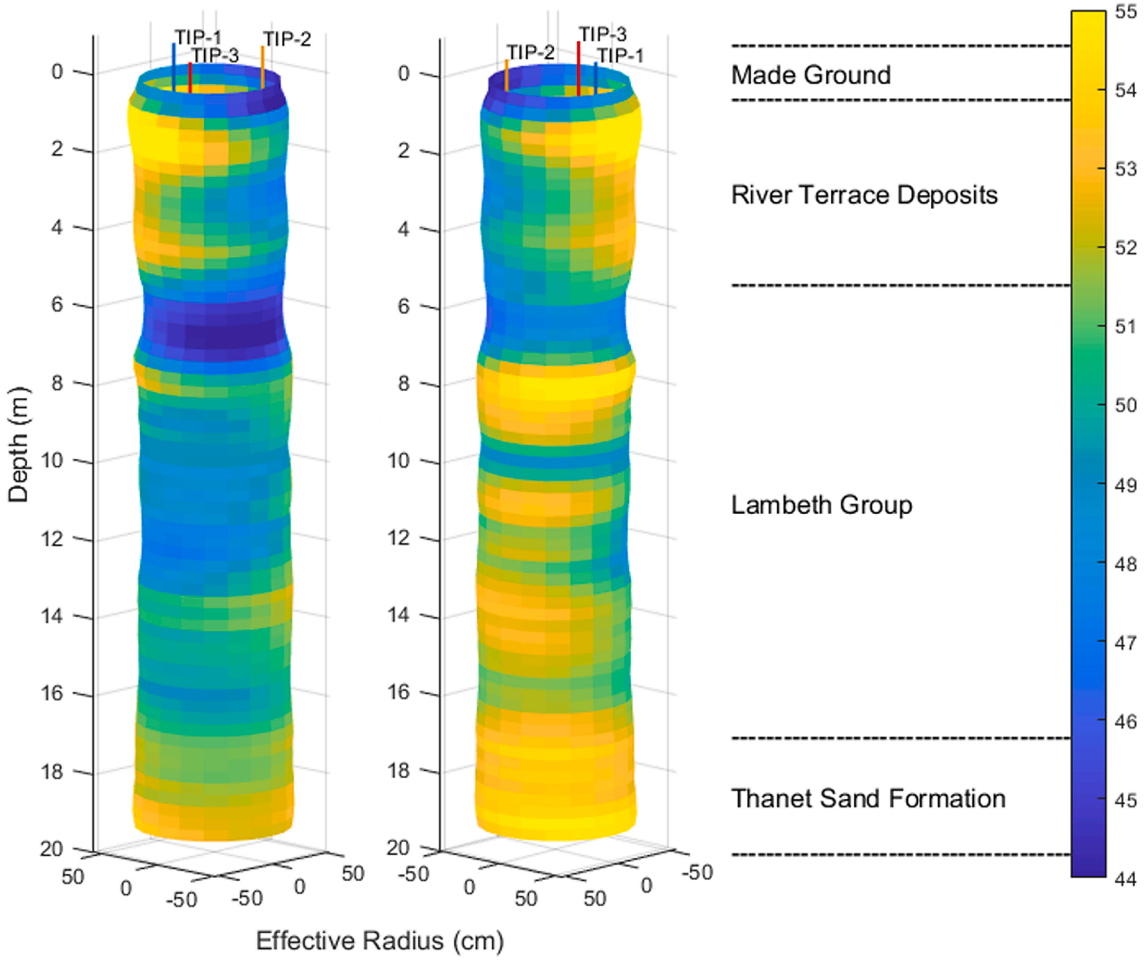

Fig. 15. Predicted pile 3D shape.

Table 7
Pile cross-section area comparison.

Depth m	Calculated Effective Radius cm	Calculated Effective Area m^2	Calculated Pile Average Area m^2	Pile Design Cross-sectional Area m^2	Construction Area Loss Percentage %	Actual Area Loss Percentage %
2.8	0.50	0.78	0.81	0.64	**3.8**	**2.4**
5.8	0.47	0.68	0.81	0.64	**18.1**	**7.1**
9.4	0.49	0.71	0.81	0.64	**8.7**	**7.1**

Table 8
Sonic logging classification and specialist sub-contractor evaluation criteria.

Classification	Increase in FAT	And/Or	Reduction in Energy
Satisfactory	0–10 %	And	less than 6 dB
Observation[1]	11–20 %	Or	6–9 dB
Flaw[2]	21–30 %	Or	9–12 dB
Defect[3]	>31 %	Or	>12 dB

[1] Observation: not normally detrimental but taken into consideration for overall assessment.
[2] Flaws: to be addressed if present in more than half profiles. Flaws present over the entire cross-section normally require redesign, repair or replacement.
[3] Defects: to be addressed if present in more than one profile.

from 43 to 57 cm. The shape of the lower half pile is relatively consistent around 51 cm in radius. Using the information obtained from the 3D shape, the volume of the concrete pile is calculated as 16.15 m^3, which is very close to the reported concrete consumption of 15.28 m^3.

3.5. Cross-section area loss and integrity analysis

Through the calculation results above, the pile effective cross-section area along the shaft can be obtained. As the pile cross-section area is related to pile bearing capacity, it is worthwhile to validate the calculation results with pile design values. Three different designed inclusions were installed inside and outside the pile reinforcement cage at depths of 2.8 m, 5.8 m and 9.4 m.

Table 7 compares the pile predicted and design cross-section areas at the three defect zones. At 2.8 m depth, sandbags accounting for 2.4 % of the calculated average cross-sectional area were installed on the reinforcement inside the concrete cover. The prediction shows a slightly higher cross-section loss of 3.8 % of the calculated average area. At 5.8 m and 9.4 m depth, the designed inclusions are inside the reinforcement cage, one in the centre of the concrete core and the other near the cage, and each of them accounts for 7.1 % of the calculated average area. The

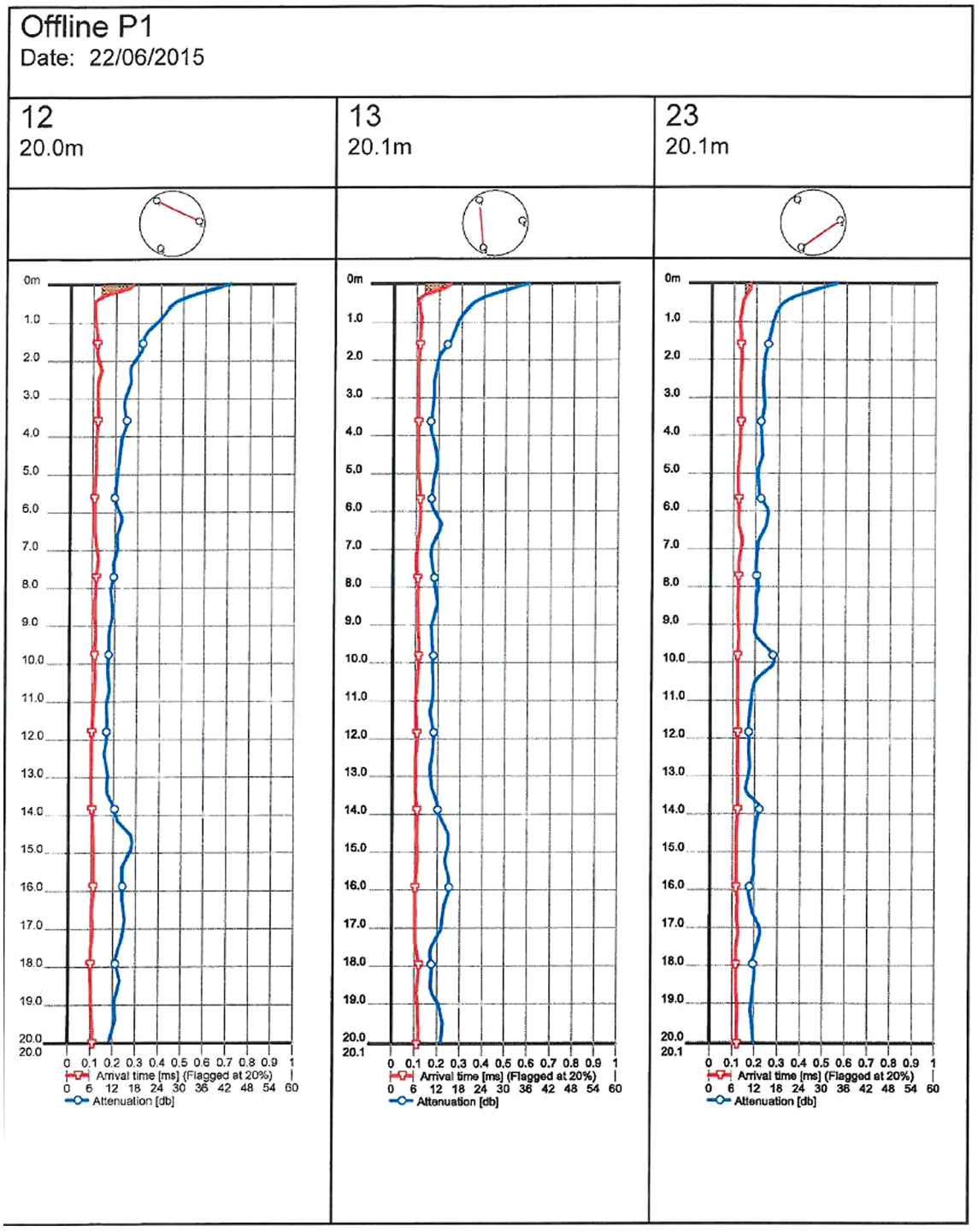

Fig. 16. Crosshole sonic logging results.

prediction results indicate area losses of 18.1 % and 8.7 %. This shows that while the effective radius method can point to the presence of anomalies within the reinforcement cage, it is less reliable in assessing their size compared to the detailed 2D Finite Element analyses proposed by Sun et al. [31]. However, this simple method can calculate the pile effective radius and plot the 3D shape of the pile quickly, providing an excellent scan tool that can point to areas of concern within the pile that needs further analysis. The method could provide an accurate prediction of the effective cross-sectional area for defects near the reinforcement cage – but is less reliable for central inclusions. The existing defect would reduce the effective area and thereby affect the pile quality. This method can be used to locate defective cross-section and evaluate pile integrity.

4. Comparison with the crosshole sonic logging data

A crosshole sonic logging (CSL) test was performed on the same trial pile to compare with the thermal integrity testing method. The CSL method is one of the most commonly used integrity test method in deep foundations and can be extended to diaphragm walls. The method is also known as ultrasonic crosshole testing as specified in the ASTM Standard D6760-16 [3].

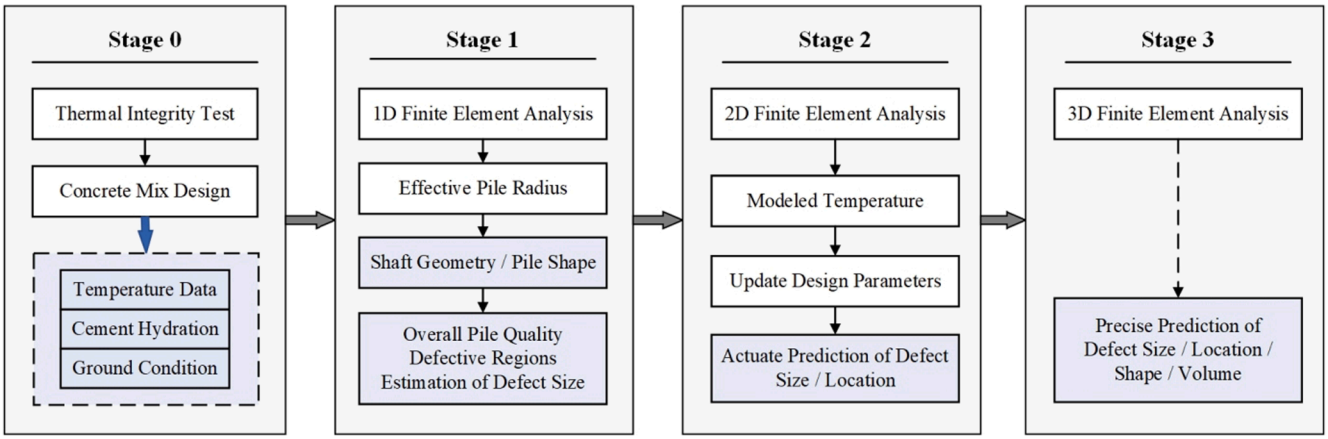

Fig. 17. Updated data interpretation framework.

It measures the first arrival time (FAT) and the energy attenuation of the sonic wave between parallel tubes inside the deep concrete foundations. Access tubes or ducts need to be installed inside the piles during construction. After construction, probes are sunk in the access tubes; the transmitter probe sends a signal pulse into the surrounding concrete, and the receiver probe measures its corresponding intensity as well as the travel time.

The principle of the test method is that the velocity of the ultrasonic wave depends on the properties of the transmission media together with its own wavelength. Concrete density and element geometry affect the pulse speed and pulse energy attenuation. A general relationship between concrete properties and pulse speed/attenuation has been developed by previous researchers [10,19]. Any fractures or weak zones inside the concrete piles will increase the first arrival time (FAT) and reduce the pulse energy.

The performed sonic logging was evaluated based on the first arrival time (FAT) and signal attenuation, with the quantitative evaluation criteria utilised by the specialist sub-contractor as outlined in Table 8. Piles with less than 10 % FAT increase and 6 dB attenuation are classified as satisfactory. Only those with >30 % FAT increase and 12 dB attenuation are regarded as major defects.

The CSL test was carried out using a Cross Hole Ultrasonic Monitor (CHUM) equipment set with three access tubes installed on the reinforcement cage. Thus, three sets of data were obtained, which are presented in Fig. 16. The red lines represent the first arrival times (FAT) which were around 0.1 ms for all three profiles. The blue lines represent the energy attenuation between the transmitter probe and the receiver probe. While CHUM analysis gave a 'satisfactory' classification for the trial pile, the following can be observed from the traces in Fig. 16.

- Inclusion 1 was not detected as it was positioned outside the cage (CSL can only evaluate the defects inside reinforcement cages and between access tubes);
- At Inclusion 2 location, all three profiles show a slight reduction in energy about 1to 2 dB, but FAT does not change at all;
- Neither FAT increase nor energy attenuation can be viewed at the Inclusion 3 location.

It is known that the inclusion 2 and 3 accounted for 9 % (each) of the designed cross-section area were designed in the pile. However, none of them were detected by CSL method, and the pile was evaluated as satisfactory despite two major defects in the middle of the concrete body. This is an example of the challenging nature of assessing pile integrity using CSL.

Compared with the crosshole sonic logging test presented above, the thermal integrity testing method can provide more detailed information about the pile integrity and detect anomalies with higher accuracy. This is promising, however, more field studies should be undertaken with various pile designs and more complex ground conditions. In addition, it is suggested that, for thermal integrity testing, (1) at least four temperature cables be installed on each test pile in order to compare the shaft condition on opposite sides; (2) temperature data collection should begin before concrete casting and end at least 40 h after concreting; (3) ground conditions including, soil stratigraphy and ground temperature, should be accurately recorded for more precise data interpretation.

5. Conclusions and recommendations

The need for better integrity tests for cast-in-situ pile is evident from a review of literature and industry practice. Thermal integrity testing, which employs temperature change induced by hydration heat as a measurement of integrity, is a promising technique.

This paper presented a case study on a CFA trial pile with engineered inclusions tested by this new technique. The key contribution of this paper is the development of a 1D finite element model that considers appropriate concrete mix and soil properties to establish a linear relationship between maximum temperature and effective pile radius. Using the linear relationship, the effective pile radii along the entire shaft could obtained, and the predicted as-built 3D shape of the pile could subsequently be reconstructed. This enables the identification of the defective zones effectively. The proposed method has successfully detected all the zones where the engineered inclusions were located (regardless of their location within the pile cross-section); however, assessing the type and size of the anomalies was less reliable, particularly when the anomalies were located inside the reinforcement cage. Consequently, the reliable results in identifying anomalous zones, combined with the very fast nature of the analyses performed, makes the proposed effective radius method an ideal first step in the staged data interpretation process proposed recently in the literature [31]. It replaces the subjective nature of the Stage 1 direct observation proposed by the researchers with an objective and quantitative approach as shown in the following flowchart (Fig. 17).

Data collection (Stage 0) is followed by the effective radius method proposed in this paper (Stage 1). The Stage 1 study can provide information on overall pile quality, including shaft geometry, pile shape, and defective region. The primary benefit of the new proposed Stage 1 is that it can provide practicing engineers with crucial information about pile integrity shortly following pile installation, hence enabling them to make informed and timely decisions on pile approval, further assessment or repair.

Following the effective radius analysis in the framework, if required, Stage 2 is employed to conduct more extensive analysis in 2D space and provide an accurate prediction of defect size and location, as described in Sun et al. [31].

More details are revealed about the anomalies being investigated (including location, size and shape) at each subsequent stage. The primary advantage of this staged process is that it enables practitioners to follow a risk-based approach and decide whether or not to pursue subsequent stages of construction depending on the results they get at the end of each stage.

The work presented in the paper highlighted the serious shortcomings of the Crosshole Sonic logging (CSL) which is commonly used in industry. In addition to not being able to detect Inclusion 1 (as it was outside the cage) the CSL method did not detect any significant change in either energy reduction or first arrival time at the locations of Inclusions 2 and 3 despite both of them being inside the reinforcement cage. In comparison, thermal integrity testing combined with a rigorous interpretation framework provides a significantly more reliable alternative.

CRediT authorship contribution statement

Qianchen Sun: Conceptualization, Methodology, Software, Validation, Investigation, Writing – original draft, Writing – review & editing, Visualization. **Mohammed Z.E.B. Elshafie:** Supervision, Funding acquisition, Conceptualization, Methodology, Writing – review & editing. **Chris Barker:** Resources. **Anthony Fisher:** Resources. **Jennifer Schooling:** Funding acquisition, Resources. **Yi Rui:** Methodology, Writing – original draft.

Declaration of Competing Interest

The authors declare that they have no known competing financial interests or personal relationships that could have appeared to influence the work reported in this paper.

Acknowledgement

The authors would like to acknowledge the support from Ove Arup & Partners Ltd and Cementation Skanska Ltd. The research has received support from the grant EP/N021614/1 (CSIC Innovation and Knowledge Centre Phase 2), Innovate UK grant 920035 (Centre for Smart Infrastructure and Construction), and the Construction Innovation Hub grant RG96631 (Centre for Digital Built Britain, University of Cambridge). This work is also performed in the framework of ITN-FINESSE, funded by the European Union's Horizon 2020 research and innovation program under the Marie Skłodowska-Curie Action grant agreement n° 722509.

This research has received support from the Centre for Digital Built Britain's (CDBB) at the University of Cambridge which is within the Construction Innovation Hub and is funded by UK Research and Innovation through the Industrial Strategy Fund.

References

[1] Ashlock JC, Fotouhi MK. Thermal integrity profiling and crosshole sonic logging of drilled shafts with artificial defects. In: Geo-Congress 2014: Geo-characterization and Modeling for Sustainability; 2014. p. 1795-1805.
[2] ASTM D7949-14, Standard Test Methods for Thermal Integrity Profiling of Concrete Deep Foundations, ASTM International, West Conshohocken, PA, 2014, www.astm.org.
[3] ASTM. Standard test method for integrity testing of concrete deep foundations by ultrasonic crosshole testing. Designation D 6760-16; 2016.
[4] Bica AVD, Prezzi M, Seo H, Salgado R, Kim D. Instrumentation and axial load testing of displacement piles. Proc Inst Civil Eng - Geotech Eng 2014;167(3):238–52.
[5] Birkhoff G, Garabedian HL. Smooth surface interpolation. J Math Phys 1960;39(1–4):258–68.
[6] Boeckmann AZ, Loehr JE. Evaluation of thermal integrity profiling and crosshole sonic logging for drilled shafts with concrete defects. Transp Res Rec 2019;2673(8):86–98.
[7] Brown DA, Turner JP, Castelli RJ, Americas PB. Drilled shafts: Construction procedures and LRFD design methods (No. FHWA-NHI-10-016). United States. Federal Highway Administration; 2010.
[8] Cameron G, Chapman T. Quality assurance of bored pile foundations. Ground Eng 2004;37(2):35–40.
[9] Camp III WM, Holley DW, Canivan GJ. Crosshole sonic logging of South Carolina drilled shafts: a five year summary. In: Contemporary Issues In Deep Foundations; 2007. p. 1-11.
[10] Chernauskas LR, Paikowsky SG. Defect detection and examination of large drilled shafts using a new cross-hole sonic logging system. In Performance Confirmation of Constructed Geotechnical Facilities; 2000. p. 66-83.
[11] De Schutter G, Taerwe L. General hydration model for Portland cement and blast furnace slag cement. Cem Concr Res 1995;25(3):593–604.
[12] De Schutter G, Taerwe L. Degree of hydration-based description of mechanical properties of early age concrete. Mater Struct 1996;29(6):335–44.
[13] Garber D. Ground source heat pump system models in an integrated building and ground energy simulation environment. PhD Dissertation, University of Cambridge; 2014.
[14] Iskander M, Roy D, Ealy C, Kelley S. Class-A prediction of construction defects in drilled shafts. Transp Res Rec 2001;1772(1):73–83.
[15] Johnson KR. Temperature prediction modeling and thermal integrity profiling of drilled shafts. In: Geo-Congress 2014: Geo-characterization and Modeling for Sustainability; 2014. p. 1781-1794.
[16] Jones WC, Wu Y. Experiences with cross-hole sonic logging and concrete coring for verification of drilled shaft integrity. In: Proceedings of the GEO Construction Quality Assurance/Quality Control Technical Conference; 2005. p. 376–87.
[17] Kim KH, Jeon SE, Kim JK, Yang S. An experimental study on thermal conductivity of concrete. Cem Concr Res 2003;33(3):363–71.
[18] Lehane BM, Jardine RJ. Displacement-pile behaviour in a soft marine clay. Can Geotech J 1994;31(2):181–91.
[19] Li DQ, Zhang LM, Tang WH. Reliability evaluation of cross-hole sonic logging for bored pile integrity. J Geotech Geoenviron Eng 2005;131(9):1130–8.
[20] McKinley S, Levine M. Cubic spline interpolation. College Redwoods 1998;45(1):1049–60.
[21] Michiel H. Spline interpolation. Encyclopedia of Mathematics, Springer; 2001.
[22] Mullins G. Advancements in Drilled Shaft Construction, Design, and Quality Assurance: The Value of Research. Int J Pavement Res Technol 2013;6(2).
[23] Mullins G, Johnson K. Optimising the use of the thermal integrity system for evaluating auger-cast piles; 2016.
[24] Mullins G, Winters D. Infrared thermal integrity testing quality assurance test method to detect drilled shaft defects (No. WA-RD 770.1). Washington (State). Dept. of Transportation. Office of Research and Library Services; 2011.
[25] Mullins G, Kranc SC, Johnson K, Stokes M, Winters D. Thermal integrity testing of drilled shafts; 2007.
[26] O'Neill MW, Sarhan HA. Structural resistance factors for drilled shafts considering construction flaws. In: Current Practices and Future Trends in Deep Foundations; 2004. p. 166-185.
[27] Piscsalko G, Likins GE, White B. Non-Destructive Testing of Drilled Shafts-Current Practice and New Method. Proceedings from the International Bridge Conference Pittsburg. 2013.
[28] Randolph MF. Science and empiricism in pile foundation design. Géotechnique 2003;53(10):847–75.
[29] Rui Y, Kechavarzi C, O'Leary F, Barker C, Nicholson D, Soga K. Integrity testing of pile cover using distributed fibre optic sensing. Sensors 2017;17(12):2949.
[30] Schoen DL, Canivan GJ, Camp III WM. Evaluation of Thermal Integrity Profiling (TIP) Methods–Probe, Embedded Wire and Wire Suspended in CSL Tubes. In: IFCEE 2018; 2018. p. 550-560.
[31] Sun Q, Elshafie M, Barker C, Fisher A, Schooling J, Rui Y. Thermal integrity testing of cast in situ piles: An alternative interpretation approach. Struct Health Monit 2020;1475921720960042.
[32] Tomlinson M, Woodward J. Pile design and construction practice. CRC Press; 2014.
[33] White B, Nagy M, Allin R. September). Comparing cross-hole sonic logging and low-strain integrity testing results. In: Proceedings of the Eighth International Conference on the Application of Stress Wave Theory to Piles; 2008. p. 471–6.